Molecular Cell, Volume *35*

Supplemental Data

Single-Molecule Analysis Reveals Differential Effect of ssDNA-Binding Proteins on DNA Translocation by XPD Helicase

Masayoshi Honda, Jeehae Park, Robert A. Pugh, Taekjip Ha, and Maria Spies

Supplemental Experimental Procedures

Fluorescence Polarization Anisotropy (FPA) –binding assays.

We used FPA to assess the ssDNA binding affinity of RPA1 and RPA2 under the conditions used for the single molecule FRET assays **(Figure S6A and S9B)**. 5FL-22 (1 nM) was used as a fluorescently-labeled ssDNA substrate. The reaction mixtures contained 50 mM Tris-HCl pH 7.5, 3 mM $MgCl_2$, 1 mM DTT and 100 μg/ml BSA. Titrations were carried out at 25 °C using Cary Eclipse Fluorescence Spectrophotometer (Varian). The initial FPA values for the DNA substrate alone were recorded followed by additions of increasing concentrations of RPA1 or RPA2. Fluorescein was excited at 490 nm, and its emission was recorded at 518 nm. Titrations of the proteins were carried out until no additional change in FPA was observed.

Ensemble FRET assay.

The ssDNA binding properties of Cy5 labeled RPA1 and RPA2 were examined by monitoring FRET between DNA-linked Cy3 (donor) and Cy5 (acceptor) incorporated into RPAs (Figure S9B). Fluorescence measurements were carried out using Cary Eclipse fluorescence spectrophotometer (Varian) at 25°C under the same reaction conditions as described above for the FPA binding assay. One nM 3Cy3-22 oligo was used as a DNA substrate. Following Cy3 excitation at 530 nm, emission at 565 nm (Cy3 emission) and 660 nm (Cy5 emission) was recorded simultaneously. The reactions were allowed to equilibrate upon addition of each protein aliquot. The FRET efficiency was calculated as:

$$FRET = \frac{4.2 * I_{Cy5}}{4.2 * I_{Cy5} + 1.7 * I_{Cy3}},$$

where I_{Cy5} is the averaged acceptor intensity, I_{Cy3} is the averaged donor intensity, 4.2 and 1.7 are correction factors for the donor and acceptor fluorescence, respectively. Measurements taken over 2 minutes of a stable signal were averaged to produce each data point.

Streptavidin Displacement Assays.

DNA translocation by XPD in bulk experiments was observed using streptavidin displacement assays (Morris and Raney, 1999). We have previously demonstrated the ability of XPD helicase to displace streptavidin from naked ssDNA (Pugh et al., 2008). Here, similar assays were carried out in the presence of RPA1 or RPA2 proteins **(Figure S6B)**. The ^{32}P-labeled oligonucleotide biotinylated at the 3'-end, 3Bio-40, (10 nM molecules) was incubated with 300 nM streptavidin in the reaction buffer containing 20 mM Tris-HCl, pH 7.5, 3 mM $MgCl_2$, 1 mM DTT and 5 mM ATP for 5 minutes followed by the addition of 6 μM biotin. RPA1 or RPA2 proteins were then added to a final concentration of 100 nM. Aliquots corresponding to zero time points were pulled and the reactions were initiated by addition of 50 nM XPD. The reactions were stopped at the indicated time points by adding an equal volume of quench solution containing 0.6% SDS and 200 mM EDTA. The reaction products were separated by electrophoresis on a 15% (19:1) native polyacrylamide gel, visualized and quantified using a Storm 840 Phosphorimager (Molecular Dynamics) and Image Quant software.

Table S1

Oligonucleotides used in this study

NAME	SEQUENCE
5Cy3-42	5’ – (Cy3)-GGATGGCTTAGAGCTTAATTCCTTTTTTTTTTTTTTTTTTTT-(bio) – 3’
3Cy3-42	5’– (bio)-TTTTTTTTTTTTTTTTTTTTGGAATTAAGCTCTAAGCCATCC-(Cy3) –3’
3Cy3-32	5’– (bio)-TTTTTTTTTTGGAATTAAGCTCTAAGCCATCC-(Cy3) –3’
3Cy3-22	5’– (bio)-GGAATTAAGCTCTAAGCCATCC-(Cy3) –3’
5FL-22	5’ (Fluorescein-T) GCCTCGCTGCCGTCGCCAGCGT 3’
3Bio-40	5’ -TTTTTTTTTTTTTTTTTTTTGCACTGGCCGTCGTACTGGG-(bio) –3’
5Cy3-22	5’-(Cy3)-GCAATTAAGCTCTAAGCCATCC-3’
3Cy3-27	5’– TGGCGACGGTCGCGAGGTTTTTTTTTT-(Cy3) –3’
3Cy3-58	5’– TGGCGACGGTCGCGAGGTTTTTTTTTTTTTTTTTTTTTTTTTTTT TTTTTTTTTTTT-(Cy3) –3
3Cy3-86	5’– TGGCGACGGTCGCGAGGTTTTTTTTTTTTTTTTTTTTTTTTTTTT TTTTTTTTTTTTTTTTTTTTTTTTTTTTTT-(Cy3) –3

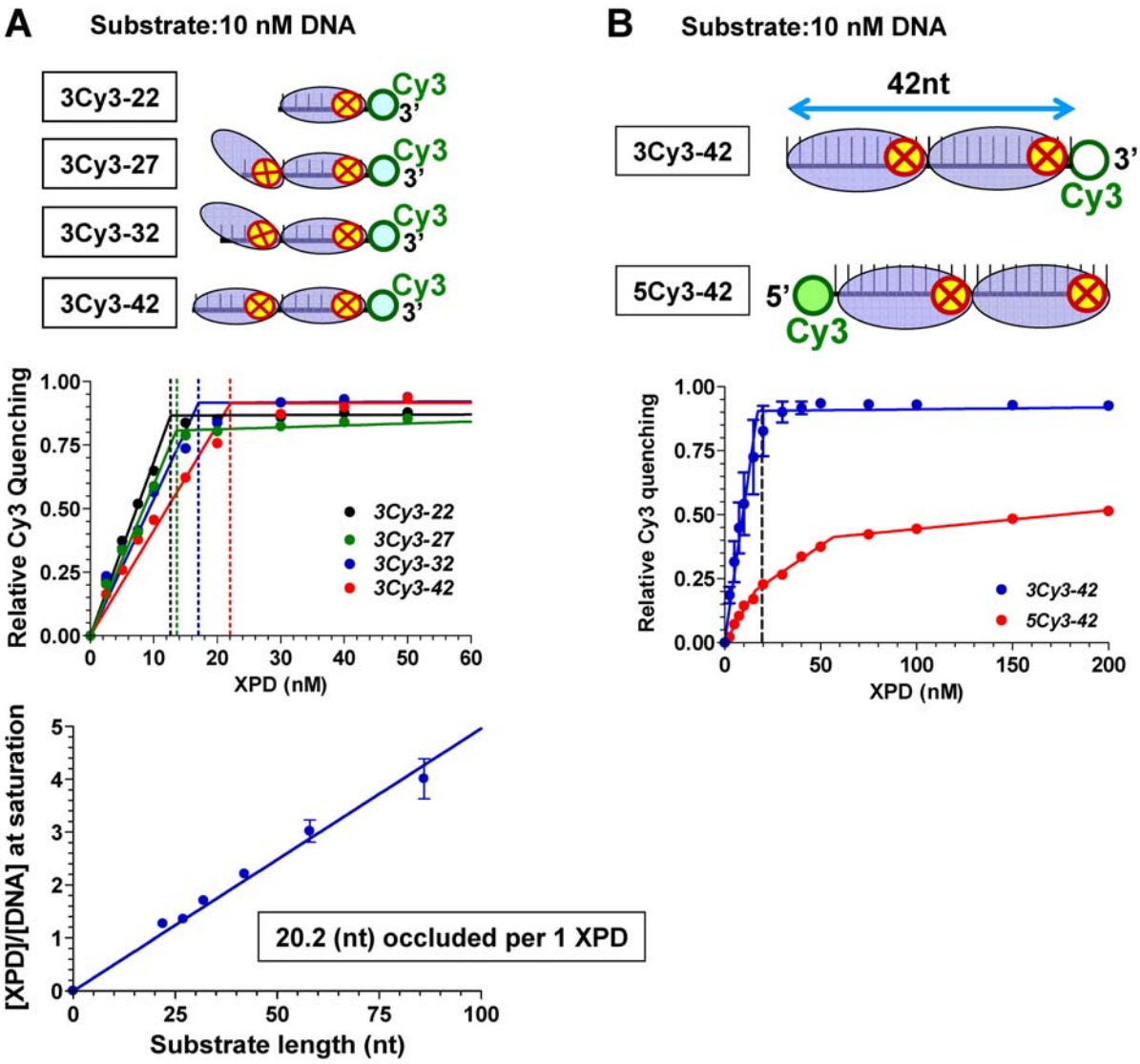

Figure S1. The FeS cluster of XPD helicase is located closer to the 3'-end of the occluded 20 nucleotides ssDNA

(A) Binding of the XPD helicase to the Cy3-labeled oligonucleotides of different lengths was analyzed under the stoichiometric binding conditions to define the binding site size of XPD. Increasing amounts of XPD helicase were titrated into the reaction mixture containing 10 nM (molecules) of each of the substrates depicted above the graph. The assays were carried out under the stoichiometric binding conditions (i.e. the DNA concentration was several fold higher than K_d for ssDNA binding by XPD helicase). Accordingly, the quenching signal increased linearly with increasing XPD concentration until the saturation was achieved. All binding isotherms were fitted to two segment lines where the break point defines the number of XPD molecules bound to each substrate at saturation. Lower panel shows quantification of the ssDNA binding site size of XPD, using the DNA substrates depicted in the top panel, 5Cy3-58 and 5Cy3-86 (data not shown) where stoichiometric amounts of XPD were plotted

as a function of the oligonucleotide length. The linear regression analysis indicated that upon binding to ssDNA, XPD occludes approximately 20.2 nt. (B) XPD binding to the oligonucleotide where Cy3 fluorophore was positioned at the 3'-end yielded higher quenching magnitude (blue circles and line) compared to the substrate containing Cy3 label at the 5'-end. This suggests that the FeS cluster is located closer to the 3- end of occluded sequence than to the 5' end. XPD binding to a 42-mer oligonucleotide decorated with Cy3 dye at the 5'-end (red) yielded more complex quenching pattern: the quenching magnitude linearly increased with increasing concentration of XPD until 2 XPD molecules were bound per 1 42-mer ssDNA; after that the quenching signal did not saturate immediately, but continued to increase. These data not only confirm that the FeS cluster is farther from the 5'-end than from the 3'-end, but also suggest the existence of the two distinct concentration-dependent DNA-binding modes in which ssDNA may be bound in one or both ssDNA binding sites of XPD helicase.

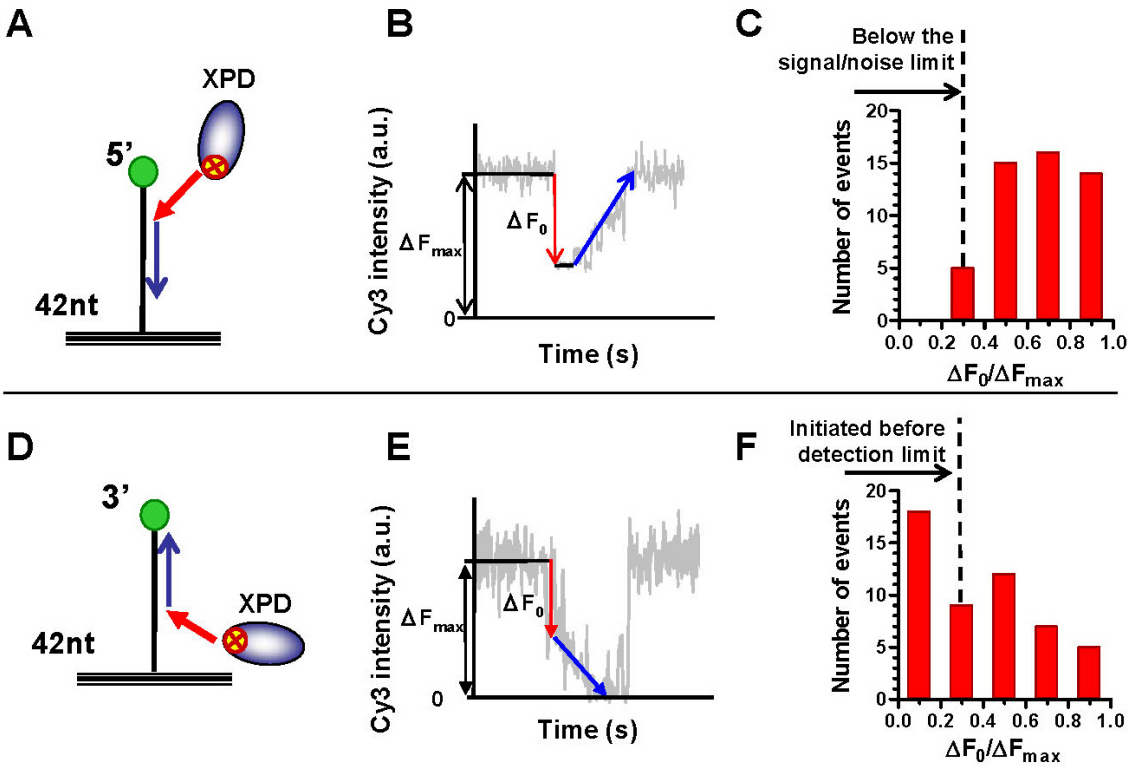

Figure S2. Binding and initiation sites for XPD are uniformly distributed along ssDNA

(A) Schematic depiction of the immobilized ssDNA (42mer) with Cy3 at the 5'-end. Cy3 fluorescence intensity abruptly decreased as result of XPD binding and then gradually recovered when the helicase translocated away from the dye in the 5' $\rightarrow$ 3'direction. (B) Schematic representation for the calculation of the initial quenching magnitude ($\Delta F_0/\Delta F_{max}$) for the individual trajectories. Initial drop in Cy3 fluorescence was attributed to binding of XPD at a distance from the dye. (C) Individual initial quenching magnitudes, which corresponded to the distribution of initial sites occupied by XPD helicase upon binding, were binned in 20% intervals of the fluorescence change and plotted as a histogram. The small fraction of events with initial quenching magnitude below 0.3 likely reflects binding events that are difficult to discern on the background noise. Binding events are uniformly distributed along the rest of the ssDNA suggesting that XPD did not have a preferred binding location. (D-F) Are analogous to A-C except ssDNA (42mer) containing Cy3 at the 3'-end was used as a substrate. In contrast to **C**, a high frequency of translocation events had initial quenching magnitude less than 0.2 in **F**. These reflect XPD binding and translocation events initiated beyond the limit of detection by Cy3 quenching.

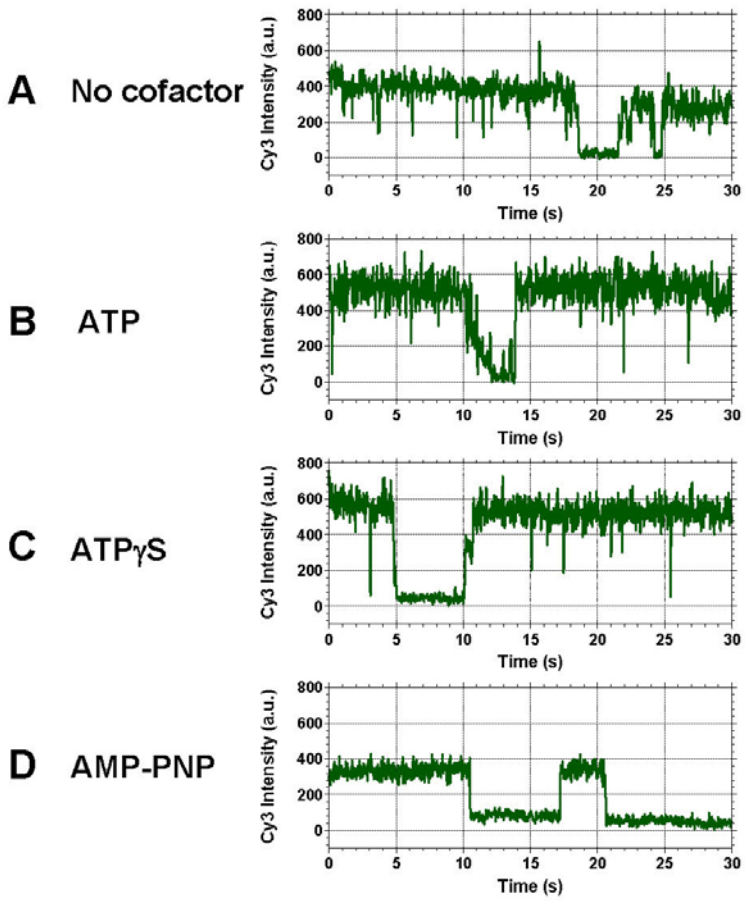

Figure S3. Observed fluorescence quenching patterns attributed to XPD translocation depend on ATP hydrolysis

Representative Cy3 fluorescence trajectories collected under different solution conditions. (A) In the absence of any nucleotide co-factor, we observed an abrupt quenching of Cy3 fluorescence (attributed to binding). This quenching was followed by a few seconds bound state and then by an abrupt fluorescence recovery (attributed to dissociation). (B) In contrast, in the presence of ATP we observed gradual quenching of Cy3 fluorescence which we attributed to XPD translocation. (C and D) Only binding was observed in the presence of the non-hydrolyzable ATP analogues.

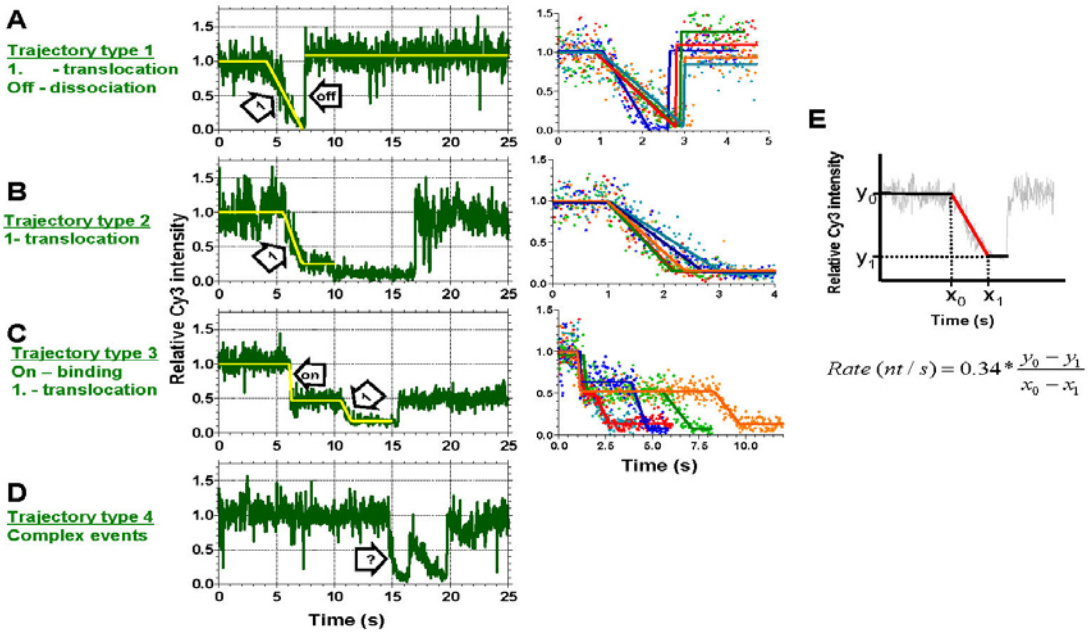

Figure S4. Classification and analysis of Cy3 trajectories coupled to XPD translocation

Individual traces that show Cy3 quenching were classified into four types of fluorescence trajectories as shown in (A-D). 42%, 22%, 30% and 6% of translocation events display characteristic patterns A, B, C and D, respectively. (A) Trajectory type 1 shows XPD translocation (indicated by arrow labeled with "1") associated with rapid dissociation from DNA (indicated by arrow labeled with "off"). Translocation rates for this type of fluorescence trajectories were calculated by fitting the experimental data to the 3 segment line shown in yellow. Five examples of the individual trajectories are shown on the right panel. (B) In the trajectory type 2 XPD translocates toward Cy3 dye and remains bound for a period of time before dissociating from ssDNA. Rate calculations were carried out by fitting trajectories of this type to a 2 segment line. (C) Trajectory type 3 shows XPD binding to ssDNA closer to Cy3 than the detection limit (indicated by arrow labeled with "on") and then translocating toward Cy3. These trajectories were fitted to a 5 segment line. (D) Trajectory type 4 exemplifyes ranslocation events which could not be categorized in any of the 3 categories described above. Most of these trajectories likely resulted from multiple translocation events due to repetitive translocation by a monomer of XPD or successive translocations of more than one helicase. The latter is more probable scenario since these events were observed more frequently at higher XPD concentrations. We did not analyze these data to ensure that all analyzed events originated from translocation of individual XPD molecules. (E) Schematic representation of the translocation rate calculation for the individual traces. Each individual translocation event was analyzed by fitting the experimental data to one of the three models shown in **A-C**. Rate (nt/s) was derived from converting slope (ΔF/s) using quenching calibration shown in Figure 1B.

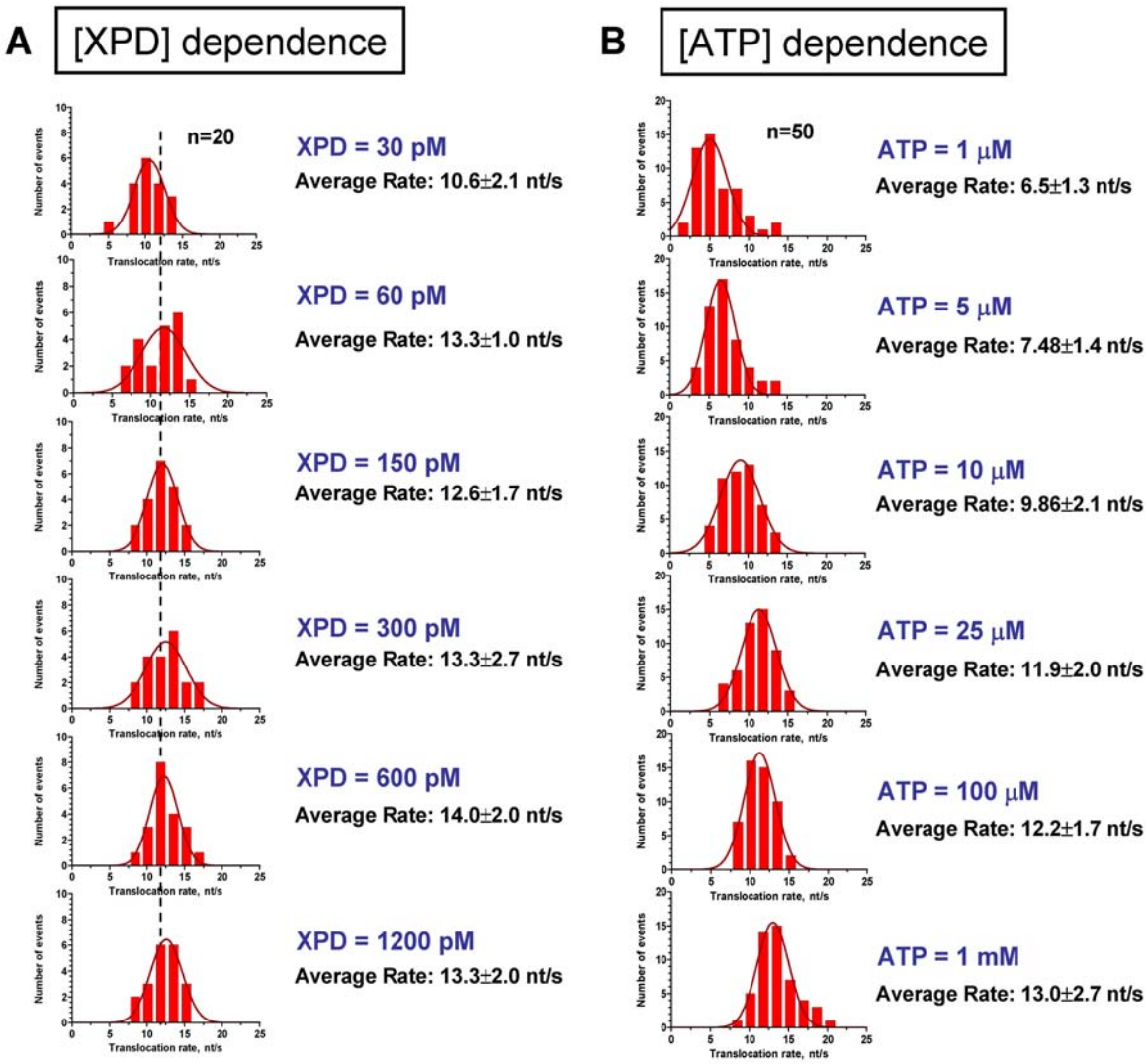

Figure S5. Distributions of the individual rates at varying XPD and ATP concentrations (summarized in Figures 2D and 2E)

Rates for individual translocation events for each condition were binned in 5% fluorescence change per second intervals, plotted and analyzed by fitting the resulting histograms to normal distributions. The mean and standard deviation were used to calculate the average translocation rate. Although, the frequency of the events continued to increase with increasing of XPD or ATP concentrations, only 20 and 50 translocation events were analyzed for each high XPD or ATP concentration, respectively. (A) Assays were carried in the presence of 1 mM ATP and indicated XPD concentrations (B) Assays were carried out in the presence of 600 pM XPD and indicated ATP concentrations.

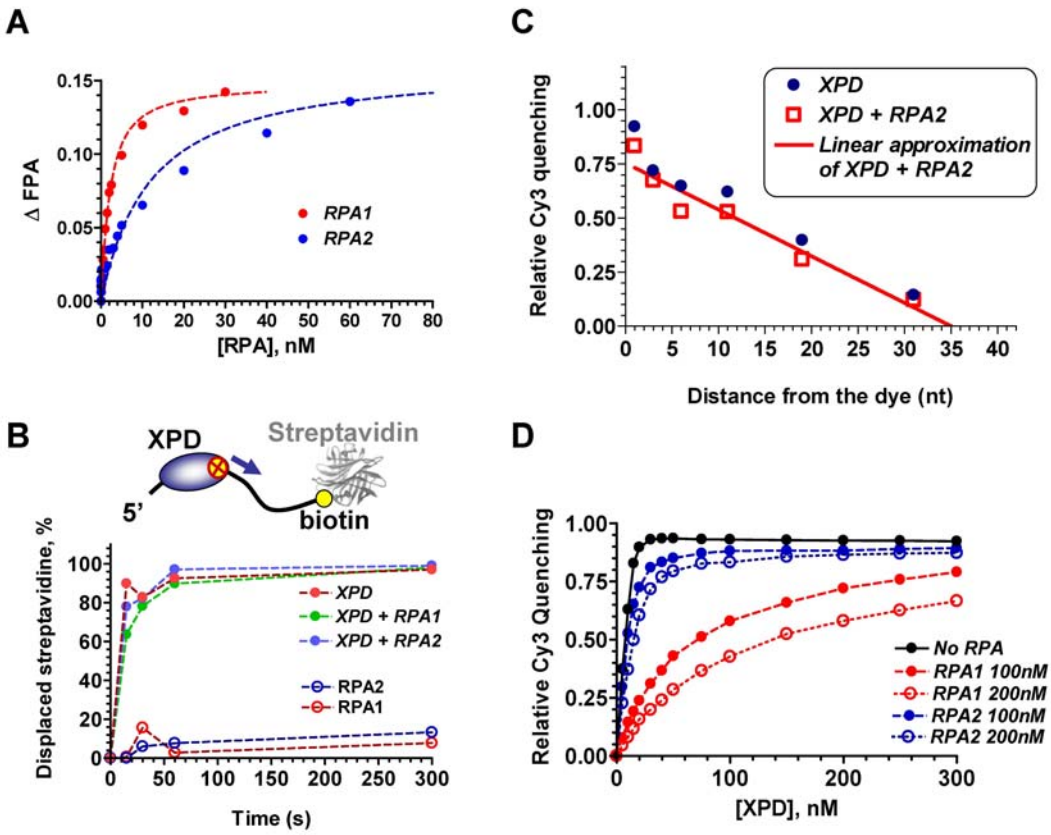

Figure S6. Effect of RPAs on XPD binding to and translocation along ssDNA

(A) Binding of RPA1 and RPA2 to ssDNA under the experimental conditions used in the single molecule experiments was analyzed by following FPA signal of the fluorescein moiety incorporated into 22 mer ssDNA. One nM (molecules) of the fluorescein-conjugated ssDNA was used in each titration. The selected substrate can accommodate one RPA1 homodimer; hence RPA1 concentration is indicated in dimers. RPA2 binds to ssDNA as monomer (22mer ssDNA can accommodate 4-5 RPA2 monomers). RPA2 concentration is therefore indicated in monomers. Under selected experimental conditions, both RPA1 and RPA2 bind to ssDNA with affinity in a low nM range. (B) XPD helicase can displace streptavidin from ssDNA coated with either RPA1 or RPA2. Streptavidin displacement assays were carried out and quantified as described in the Supplemental Experimental Procedures. (C) Calibration of Cy3 quenching performed in the presence of RPA2 resulted in the same change in Cy3 quenching magnitude as that obtained using the protein-free ssDNA. Due to the low affinity of XPD for the RPA1-coated DNA we could not achieve the stoichiometric binding conditions and therefore did not carry out calibration. (D) RPA1 inhibits XPD binding to ssDNA to a greater extent than RPA2. Effect of RPA1 and RPA2 binding on XPD-ssDNA interactions was analyzed by following XPD-dependent quenching of Cy3 fluorescence in the presence and absence of RPAs. The XPD binding titrations were carried out in the presence of indicated amounts of the ssDNA binding proteins using 10 nM 3Cy3-42 as the substrate.

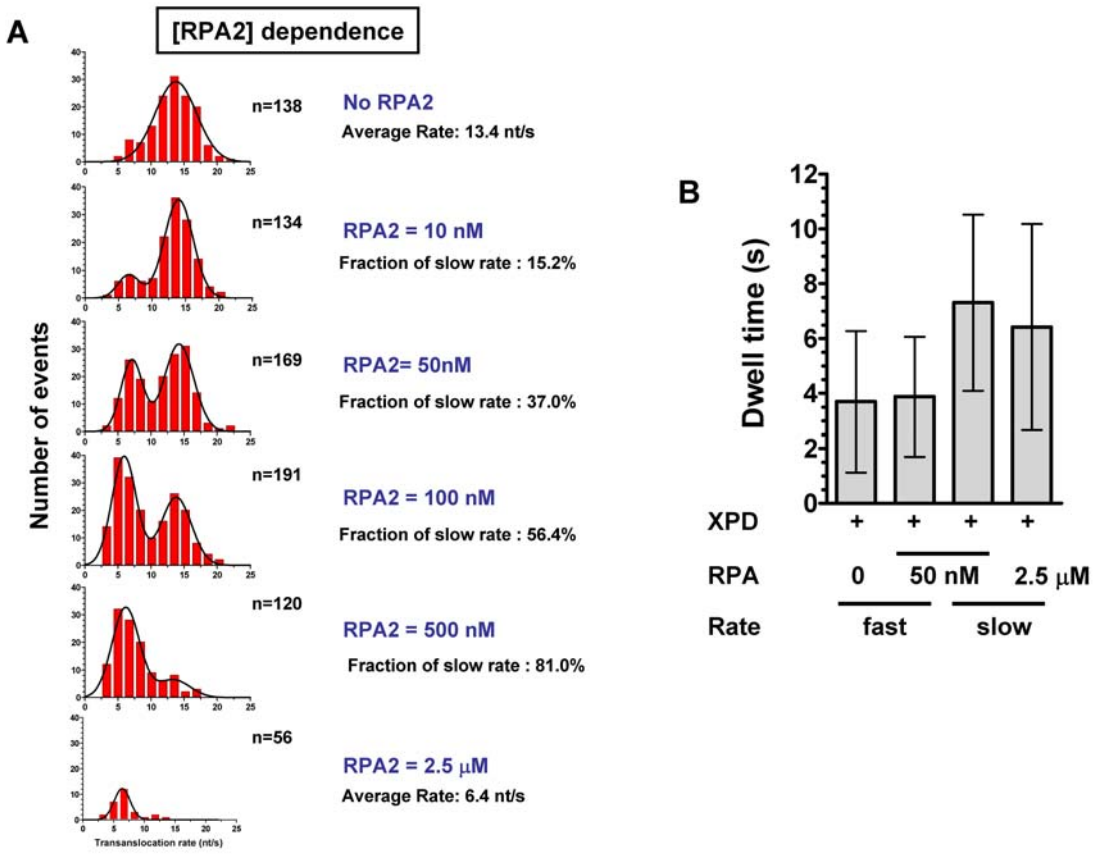

Figure S7. Fraction of slow translocating XPD molecules increases with increasing concentration of RPA2.

(A) Individual rates were binned in 5% fluorescence change per second intervals, plotted and analyzed by fitting the resulting histogram to double-normal distribution. The average and standard deviation were used to calculate the average translocation rate. The value "n" represents the total number of translocation events observed per 600 randomly selected trajectories. Assays were carried out in the presence of 1 mM ATP and 150 pM XPD. Areas under each distribution peak were used to estimate the fraction of fast and slow translocation molecules (Summarized in Figure 3D). (B) The lifetime of XPD on ssDNA increased due to RPA2. Average dwell times of 25 individual XPD translocation events in the presence of 0, 50 and 2.5 μM of RPA2 concentration were counted and plotted as a histogram. In the presence of 50 nM RPA2, dwell times for slow and first translocation rates were analyzed separately.

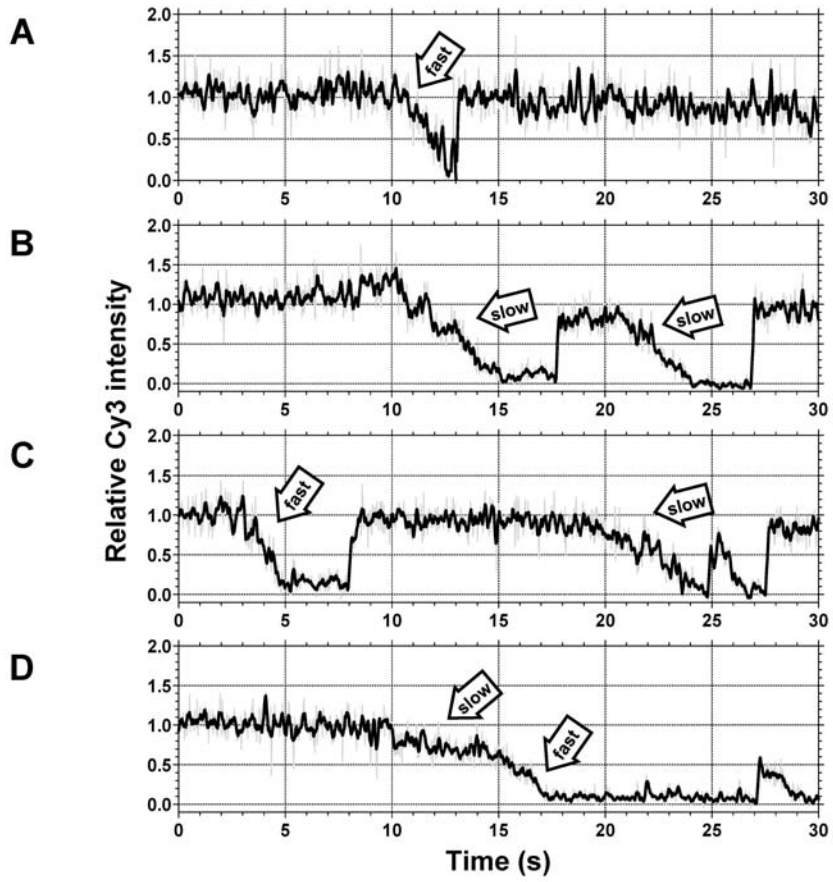

Figure S8. Representative fluorescence trajectories of XPD translocating on RPA2-coated ssDNA

(A) Trajectory type 1 shows XPD translocation with a fast rate. Cy3 fluorescence is completely quenched within 1-3 sec similar to that observed on the protein-free ssDNA and in the presence of RPA1. The event is indicated by arrow labeled with "fast". (B) Trajectory type 2 shows XPD translocation with a slower rate than normal (fast) rate, which corresponds to the second peak in the rate distribution in the presence of RPA2. In this case, complete quenching of Cy3 takes 5-10 seconds. The event is indicated by the arrow labeled with "slow". (C) Trajectory type 3 includes distinct normal and slow translocation events within the same fluorescent trajectory. Both events are indicated by arrows. (D) Trajectory type 4 exhibited biphasic behavior where the translocation of the helicase suddenly accelerates during translocation. The slow rate follows by the faster translocation. This change in the behavior may be attributed to dissociation of the RPA2 during the translocation event or overcoming of one bound RPA2 (slow phase) and continuing onto the protein-free region of ssDNA (fast phase).

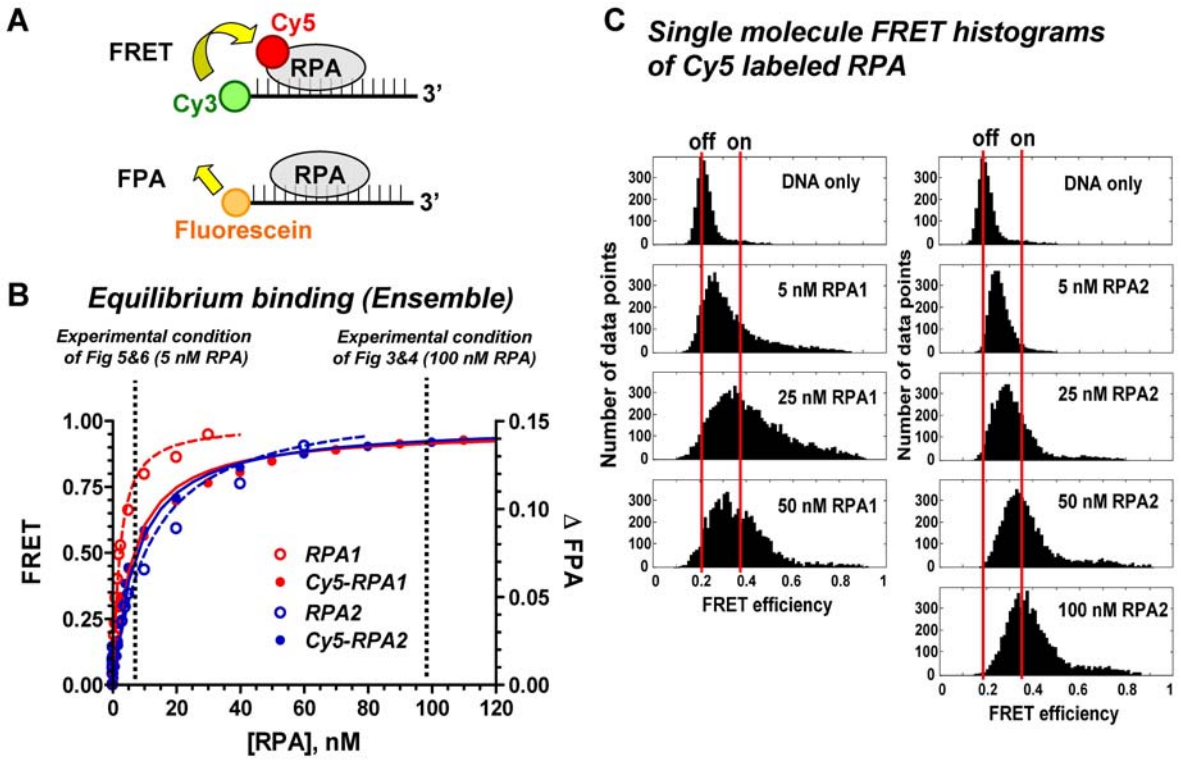

Figure S9. N-terminal labeling does not prevent RPA-binding to ssDNA

(A and B) Binding of the Cy5 labeled and unlabeled RPA to 22 nt ssDNA were compared in bulk assays using FRET between Cy5-labeled RPAs and Cy3-labeled ssDNA to evaluate binding of the labeled proteins, and the FPA signal of the fluorescein-labeled ssDNA for unlabeled proteins. Schematic depiction of FRET and FPA measurements are presented in **A**. (C) Binding of RPA proteins to the immobilized ssDNA was then confirmed by analysis of the smFRET histograms obtained after incubating immobilized 3Cy3-42 with different concentrations of ssDNA binding proteins. Emission in Cy3 and Cy5 channels upon excitation of Cy3 dye was then collected and presented as FRET signal.

Supplemental References

Morris, P. D., and Raney, K. D. (1999). DNA helicases displace streptavidin from biotin-labeled oligonucleotides. Biochemistry *38*, 5164-5171.

Pugh, R. A., Honda, M., Leesley, H., Thomas, A., Lin, Y., Nilges, M. J., Cann, I. K., and Spies, M. (2008). The iron-containing domain is essential in Rad3 helicases for coupling of ATP hydrolysis to DNA translocation and for targeting the helicase to the single-stranded DNA-double-stranded DNA junction. J Biol Chem *283*, 1732-1743.